Available online at www.sciencedirect.com
SCIENCE DIRECT®
Journal of Solid State Chemistry 178 (2005) 2237–2246
JOURNAL OF SOLID STATE CHEMISTRY
www.elsevier.com/locate/jssc

Single crystal X-ray diffraction studies on $[(CH_3)_nNH_{4-n}]_3[Sb_2Cl_9]$ ($n = 2, 3$) chloroantimonates(III) in their low-temperature ferroelectric phases—structures and phase transitions

Maciej Bujak*,[1], Ross J. Angel

Crystallography Laboratory, Department of Geosciences, Virginia Tech, Blacksburg, VA 24061, USA

Received 11 March 2005; received in revised form 18 April 2005; accepted 19 April 2005
Available online 1 June 2005

Abstract

The structures of two ferroic chloroantimonates(III): $[(CH_3)_2NH_2]_3[Sb_2Cl_9]$ (DMACA) and $[(CH_3)_3NH]_3[Sb_2Cl_9]$ (TMACA) were determined in their low-temperature phases. The structure of DMACA was investigated at 100 and 15 K, and TMACA at 15 K. The structures consist of two-dimensional inorganic layers and organic cations bound together by the N(C)–H···Cl hydrogen bonds. All of the organic cations in both compounds at all studied temperatures are ordered. There is no indication of the structural phase transition in the structure of DMACA below 242 K. The geometry and distortions of the $[SbCl_6]^{3-}$ octahedra in both compounds is discussed. The monoclinic *Pc* space group was found for both compounds: DMACA $a = 9.3590(5)$, $b = 9.0097(4)$, $c = 14.1308(7)$ Å, $\beta = 95.229(4)^\circ$, $R_1 = 0.0240$, w$R_2 = 0.0491$ and $a = 9.3132(4)$, $b = 9.0008(3)$, $c = 14.1088(5)$ Å, $\beta = 95.010(3)^\circ$, $R_1 = 0.0230$, w$R_2 = 0.0482$ at 100 and 15 K, respectively; TMACA $a = 9.8652(5)$, $b = 9.1129(4)$, $c = 15.0964(7)$ Å, $\beta = 89.988(4)^\circ$, $R_1 = 0.0239$, w$R_2 = 0.0611$ at 15 K.

Keywords: Chloroantimonates(III); Ferroic crystals; Organic–inorganic hybrid materials; Crystal structure; Phase transitions

1. Introduction

The structures of halogenoantimonates(III) and halogenobismuthates(III) with organic cations, a new group of ferroic crystals, are best described as molecular-ionic, organic–inorganic hybrid materials. They consist of organic cations within anionic inorganic frameworks. Differences in the size, symmetry and ability to form hydrogen bonds of the various possible organic cations, together with the many different possible metal-halogen atom configurations provide a rich family of compounds. The anionic structures which have been reported so far range from simple isolated $[MX_6]^{3-}$ octahedra and $[MX_5]^{2-}$ square pyramids (M—Sb^{III}, Bi^{III}; X—Cl, Br, I) through isolated units containing octahedra/square pyramids, connected by corners, edges or faces, to infinite one- or two-dimensional polyanionic structures [1–5].

The phase transition behavior and resulting physical properties of halogenoantimonates(III) and halogenobismuthates(III) with organic cations can be adjusted by the choice of organic cation and by the form of anionic structure. There appear to be two primary structural mechanisms involved in the phase transitions in these materials. At higher temperatures the molecular cations typically exhibit large reorientation motions in the solid state, which become frozen on decreasing temperature. This freezing is usually associated with changes in the hydrogen bonding scheme between the organic cation and the anionic groups which results in significant distortions of the latter [6–8]. This feedback between the two structural elements is responsible for

*Corresponding author. Fax: +1 540 231 3386.
E-mail addresses: mbujak@vt.edu, mbujak@uni.opole.pl (M. Bujak).
[1]*Permanent address*: Institute of Chemistry, University of Opole, Oleska 48, 45-052 Opole, Poland.

0022-4596/$ - see front matter © 2005 Elsevier Inc. All rights reserved.
doi:10.1016/j.jssc.2005.04.020

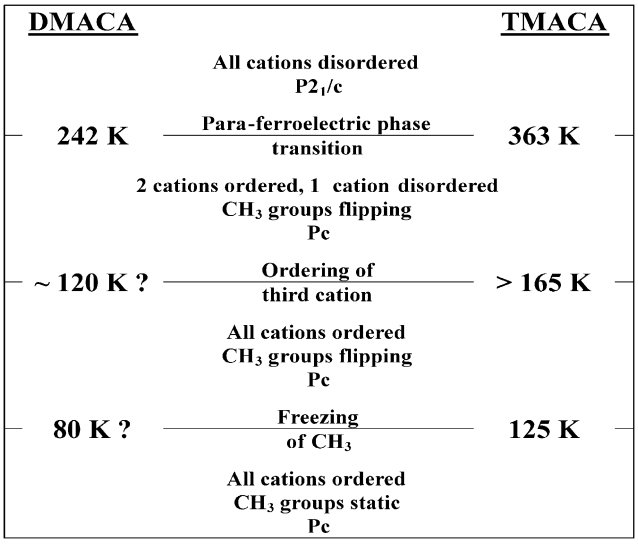

Fig. 1. A diagrammatic representation of the phase transition sequence and structural changes of DMACA and TMACA crystals as a function of temperature based upon published data and the current work. See text for details.

the complex transition situation in this family of compounds, and provides the opportunity to tailor the transition behavior and physical properties through synthesis: in different compounds transitions to ferroelectric, ferroelastic or pyroelectric phases have already been demonstrated [3,7,8 and references therein].

The most interesting from the view of technical applications are compounds with relatively small alkylammonium cations. Among them is a group containing the two-dimensional $[\{M_2X_9\}_n]^{3n-}$ layered polyanions. To this group of crystals belongs, among others, $(CH_3NH_3)_3[Sb_2Br_9]$ (MABA) and $(CH_3NH_3)_3[Bi_2Br_9]$ (MABB) [9,10] which transform at low temperatures to ferroelastic and then to ferroelectric phases [11–13]. The dimethylammonium crystal structures $[(CH_3)_2NH_2]_3[Sb_2Cl_9]$ (DMACA) and $[(CH_3)_2NH_2]_3[Sb_2Br_9]$ (DMABA) [14,15] undergo transitions at low temperatures to ferroelectric phases [16,17]. The ferroelectric trimethylammonium analogue $[(CH_3)_3NH]_3[Sb_2Cl_9]$ (TMACA) [18] shows a similar sequence of phase transitions [19,20] (Fig. 1). At higher temperatures the cations undergo rapid re-orientational motions which become ordered upon cooling, although in both DMACA and TMACA structures this is a two-step process with two cations becoming ordered at the para-ferroelectric phase transition and the third becoming ordered at lower temperature without any further change in symmetry. In addition, there is also spectroscopic evidence [20–23] that at higher temperatures the methyl groups also undergo 120° flipping motions that swap the positions of the hydrogen atoms. This reorientation process only becomes frozen at temperatures below that at which all of the reorientation motions of the cations are frozen (Fig. 1) [20,22,23]. There have also been claims on the basis of infra-red and Raman spectroscopic measurements that further reductions in symmetry of both DMACA and TMACA also occur at temperatures below 150 K [24].

In order to obtain further and detailed information about structures and mechanisms of the phase transitions in these classes of compounds, and in order to determine whether further symmetry changes occur below 150 K, as suggested by Varma et al. [24], we have determined single crystal structures of DMACA and TMACA down to 15 K.

2. Experimental

2.1. Preparation of single crystals

Antimony(III) oxide (99.9%, Sigma-Aldrich), dimethylamine (40 wt% solution in water), trimethylamine (50 wt% solution in water, both Acros Organics) and concentrated hydrochloric acid (36.5–38%, EM Science) were the starting materials used for the synthesis of both compounds in similar synthetic procedures. 2.915 g (10 mmol) Sb_2O_3 dissolved in ca. 15 mL of hot concentrated HCl were treated with 3.80 mL (30 mmol) of dimethylamine and 4.10 mL (30 mmol) of trimethylamine dissolved in 2.0 mL of ca. 6 M HCl in the case of synthesis of DMACA and TMACA crystals, respectively. The solutions were heated and stirred and ca. 6 M HCl was added (synthesis of the TMACA crystals) until the precipitated products of the reactions were completely dissolved. The acid solutions were allowed to slowly evaporate at room temperature until the transparent, colorless crystals were grown.

2.2. X-ray measurements and structure determinations

Intensity data were collected on an Oxford Diffraction Xcalibur 2 diffractometer equipped with an Enhance X-ray source and a Sapphire 3 CCD detector. The Oxford Diffraction Cryojet XL and Helijet coolers were used for the measurements at 100 and 15 K, respectively. All accessible reflections were measured using the φ- and ω-scan techniques with $\Delta\omega = 1.0°$ and $\Delta t = 5$ and 15 s. The unit cell parameters were obtained from a least squares refinement of 12114, 15690 and 20389 reflections at 100, 15 K for DMACA and at 15 K for TMACA, respectively. The data were subjected to Lorentz, polarization and numerical absorption corrections [25]. The Oxford Diffraction software CrysAlis CCD and CrysAlis RED programs were used during the data collection, cell refinement and data reduction processes [25]. SHELXTL NT was used for the structure solution and refinement. All structures were solved by

Table 1
The crystal data, X-ray measurements and structure determination summary for DMACA at 100 and 15 K, and for TMACA at 15 K

	DMACA		TMACA
	100 K	15 K	15 K
Empirical formula	$C_6H_{24}Cl_9N_3Sb_2$		$C_9H_{30}Cl_9N_3Sb_2$
Formula weight	700.83		742.91
Crystal color; habit		Colorless; hexagonal-shaped plates	
Crystal size (mm^3)	$0.14 \times 0.12 \times 0.08$	$0.22 \times 0.22 \times 0.12$	$0.24 \times 0.22 \times 0.20$
Crystal system		Monoclinic	
Space group		*Pc*	
Unit cell dimensions (Å, deg)	$a = 9.3590(5)$	$a = 9.3132(4)$	$a = 9.8652(5)$
	$b = 9.0097(4)$	$b = 9.0008(3)$	$b = 9.1129(4)$
	$c = 14.1308(7)$	$c = 14.1088(5)$	$c = 15.0964(7)$
	$\beta = 95.229(4)$	$\beta = 95.010(3)$	$\beta = 89.988(4)$
Volume ($Å^3$)	1186.58(10)	1178.17(8)	1357.18(11)
Z		2	
Density (calculated) ($g\,cm^{-3}$)	1.962	1.976	1.818
Wavelength (Å)		Mo$K\alpha$, $\lambda = 0.71073$	
Absorption coefficient (mm^{-1})	3.284	3.308	2.877
F(000)	672		720
θ Range (deg)	4.14–24.99	4.15–25.00	4.07–25.00
Index ranges	$-11 \leqslant h \leqslant 11; -10 \leqslant k \leqslant 10; -16 \leqslant l \leqslant 16$		$-11 \leqslant h \leqslant 11; -10 \leqslant k \leqslant 10; -17 \leqslant l \leqslant 17$
Reflections collected/unique	16084/4122 ($R_{int} = 0.0275$)	15849/4085 ($R_{int} = 0.0240$)	18064/4690 ($R_{int} = 0.0268$)
Observed reflections [$I > 2\sigma(I)$]	3972	4008	4630
Data/parameters	4122/253	4085/253	4690/300
Goodness of fit on F^2	1.120	1.169	1.285
Final *R* indices [$I > 2\sigma(I)$][a]	$R_1 = 0.0230$, w$R_2 = 0.0487$	$R_1 = 0.0226$, w$R_2 = 0.0480$	$R_1 = 0.0232$, w$R_2 = 0.0599$
R indices (all data)[a]	$R_1 = 0.0240$, w$R_2 = 0.0491$	$R_1 = 0.0230$, w$R_2 = 0.0482$	$R_1 = 0.0239$, w$R_2 = 0.0611$
Absolute structure parameter	0.00	0.00	−0.047(18)
Largest diff. peak/hole ($e\,Å^{-3}$)	0.977/–0.668	1.283/–0.755	0.903/–0.778

[a] $R_1 = \Sigma||F_0| - |F_c||/\Sigma|F_0|$; w$R_2 = \{\Sigma[w(F_0^2 - F_c^2)^2]/\Sigma[w(F_0^2)^2]\}^{1/2}$.

the Patterson method. All hydrogen atoms were located in subsequent maps, refined and constrained to the same distance (SADI command of SHELXTL NC) for CH_3, NH_2^+ and NH^+ groups. Their displacement parameters were taken with coefficients 1.5 and 1.2 times larger than the respective parameters of the methyl carbon and nitrogen atoms. The structure drawings were prepared using the XP program within SHELXTL NT [26].

The crystal data and the structure determination details for DMACA at 100 and 15 K, and for TMACA at 15 K are listed in Table 1. The final atomic coordinates and equivalent isotropic displacement parameters for non-hydrogen atoms are shown in Table 2. The bond lengths, angles and the hydrogen bond geometries are presented in Tables 3 and 4. Crystallographic data (excluding structure factors) for tris(dimethylammonium) nonachlorodiantimonate(III), DMACA, at 100 and 15 K and for tris(trimethylammonium) nonachlorodiantimonate(III), TMACA, at 15 K have been deposited at the Cambridge Crystallographic Data Centre as supplementary publication nos. CCDC 265842, 265843 and 265844. Copies of the data can be obtained, free of charge, on application to the Director, CCDC, 12 Union Road, Cambridge CB2 1EZ, UK (Fax: 44 1223 336-033; e-mail: deposit@ccdc.cam.ac.uk).

3. Results and discussion

3.1. Low-temperature structures of DMACA and TMACA

Both of the compounds, DMACA and TMACA, contain two-dimensional $[\{Sb_2Cl_9\}_n]^{3n-}$ polyanionic layers between and within which are located several symmetrically distinct di- and trimethylammonium cations (Fig. 2). At higher temperatures these cations are dynamically disordered. Upon cooling the cations become ordered, giving rise to a sequence of structural changes as well as a para-ferroelectric phase transition from the centrosymmetric $P2_1/c$ space group to the polar *Pc* space group. Further phase transitions that do not give rise to symmetry changes have also been reported on the basis of physical property measurements and a further reduction in symmetry of the structure was suggested by Varma et al. [24]. The results of this work now show that both compounds show analogous behavior down to 15 K, with the temperatures of the

Table 2
Atomic coordinates ($\times 10^4$) and equivalent isotropic displacement parameters ($Å^2 \times 10^3$) for non-hydrogen atoms of DMACA at 100 and 15 K, and of TMACA at 15 K

Atom	x	y	z	U_{eq}[a]
DMACA, 100 K				
Sb1	3(1)	2072(1)	10(1)	15(1)
Sb2	3243(1)	7033(1)	1661(1)	15(1)
Cl1	−1500(1)	152(2)	−742(1)	25(1)
Cl2	−1275(2)	1639(2)	1542(1)	24(1)
Cl3	−1866(2)	3902(2)	−505(1)	22(1)
Cl4	1566(2)	4820(2)	1073(1)	25(1)
Cl5	1097(1)	2313(2)	−1670(1)	28(1)
Cl6	1985(2)	−337(2)	454(1)	25(1)
Cl11	5239(2)	8974(2)	2166(1)	21(1)
Cl12	4590(2)	6534(2)	322(1)	23(1)
Cl13	4548(2)	5329(2)	2732(1)	24(1)
N1A	−1893(5)	3059(5)	−2933(3)	24(1)
C1A	−2005(6)	4698(6)	−3010(4)	24(1)
C2A	−1521(7)	2345(7)	−3826(5)	35(2)
N2A	5372(5)	1246(5)	471(3)	25(1)
C3A	4984(7)	1250(9)	−553(4)	38(2)
C4A	4952(7)	2591(8)	963(6)	40(2)
N3B	1187(5)	1793(5)	3400(3)	25(1)
C5B	2525(8)	1648(9)	2942(5)	28(2)
C6B	867(10)	3329(10)	3675(6)	40(2)
DMACA, 15 K				
Sb1	3(1)	2053(1)	13(1)	8(1)
Sb2	3242(1)	7012(1)	1658(1)	8(1)
Cl1	−1503(1)	112(1)	−728(1)	13(1)
Cl2	−1285(2)	1620(2)	1549(1)	13(1)
Cl3	−1872(2)	3884(2)	−508(1)	10(1)
Cl4	1558(1)	4787(2)	1066(1)	12(1)
Cl5	1099(1)	2290(1)	−1675(1)	14(1)
Cl6	2018(1)	−349(1)	452(1)	13(1)
Cl11	5245(2)	8948(2)	2163(1)	11(1)
Cl12	4600(2)	6506(2)	316(1)	12(1)
Cl13	4546(1)	5303(1)	2732(1)	13(1)
N1A	−1883(5)	3098(5)	−2925(3)	14(1)
C1A	−2000(5)	4733(6)	−3000(4)	14(1)
C2A	−1512(6)	2381(6)	−3828(4)	18(1)
N2A	5366(4)	1206(5)	460(3)	13(1)
C3A	4983(6)	1265(7)	−578(4)	17(1)
C4A	4953(6)	2574(7)	962(4)	18(1)
N3B	1203(4)	1794(5)	3398(3)	15(1)
C5B	2553(7)	1652(8)	2932(4)	15(1)
C6B	890(7)	3332(8)	3676(5)	20(1)
TMACA, 15 K				
Sb1	8(1)	2031(1)	2(1)	7(1)
Sb2	3023(1)	7086(1)	1715(1)	7(1)
Cl1	−1140(1)	115(1)	−795(1)	10(1)
Cl2	−1226(1)	1430(1)	1335(1)	11(1)
Cl3	−1831(1)	3785(1)	−388(1)	11(1)
Cl4	1489(1)	4392(1)	1216(1)	12(1)
Cl5	1109(1)	2821(1)	−1877(1)	11(1)
Cl6	1853(1)	−194(1)	534(1)	12(1)
Cl11	4249(1)	9123(1)	2391(1)	12(1)
Cl12	4818(1)	6718(1)	592(1)	12(1)
Cl13	4221(1)	5401(1)	2662(1)	11(1)
N1A	−1478(4)	3191(4)	−3124(3)	11(1)
C1A	−2152(5)	4669(5)	−3111(3)	11(1)
C2A	−2363(6)	2058(5)	−2681(3)	15(1)
C3A	−1124(5)	2739(5)	−4042(3)	13(1)
N2A	4510(4)	1702(5)	367(3)	11(1)
C4A	5471(6)	574(5)	16(4)	16(1)
C5A	5087(5)	2493(6)	1144(3)	13(1)
C6A	4113(5)	2751(6)	−342(3)	13(1)
N3B	1481(4)	3240(5)	3271(3)	11(1)
C7B	−21(5)	3322(6)	3340(3)	15(1)
C8B	1956(5)	1780(6)	2947(4)	15(1)
C9B	2117(6)	3629(5)	4132(3)	16(1)

[a] U_{eq} is defined as one-third of the trace of the orthogonalized U_{ij} tensor.

corresponding phase transitions and cation ordering being higher in TMACA than in DMACA (Fig. 1). The structures at 15 K have space group *Pc* with completely ordered cations and appear to be the ground-state of these compounds.

3.2. Organic cations

In the high-temperature $P2_1/c$ phases of both compounds there are two symmetrically distinct cation sites and in both compounds both of these cations are orientationally disordered. In addition, each methyl group also undergoes dynamic flipping around the three-fold axis [20–23]. The flipping of the hydrogen atoms cannot be detected by X-ray diffraction measurements, but the orientational disorder of the cation as a whole can be represented in refined X-ray structures as sets of two or three (as appropriate) partially occupied sites for C and N atoms. Upon cooling through the para-ferroelectric phase transition the symmetry is reduced from $P2_1/c$ to *Pc* and there are three symmetrically distinct cation sites in the unit-cell of each compound denoted N1A, N2A and N3B (Table 2, Fig. 2). The notation "A" indicates cations located between the inorganic layers, and "B" those within the corrugations of the layers. Within the ferroelectric phase of DMACA at 200 K (42 K below the para-ferroelectric phase transition) the cation located within the inorganic layer and one of two symmetrically independent cations located between the layers can be described as single molecules in structure refinements [27] and are therefore considered to be orientationally ordered. A similar situation was found for TMACA at room temperature, 68 K below its para-ferroelectric phase transition [28]. In this structure the N3B trimethylammonium cations located within the anionic layers possesses relatively large displacement parameters and have to be modeled as a pair of split molecules, indicating that they remain orientationally disordered while the N1A and N2A cations are ordered.

A previous structure determination [5] has shown that at 165 K the N3B cation in TMACA is ordered and it remains so at 95 K. Our data at 15 K further confirm this

Table 3
Selected bond lengths (Å) and angles (°) for DMACA at 100 and 15 K, and for TMACA at 15 K

Atoms	DMACA		TMACA
	100 K	15 K	15 K
Sb1–Cl1	2.4149(13)	2.4200(12)	2.4036(11)
Sb1–Cl2	2.5961(14)	2.5961(13)	2.4139(11)
Sb1–Cl3	2.4650(15)	2.4665(14)	2.4888(11)
Sb1–Cl4	3.1813(15)	3.1595(13)	3.1826(11)
Sb1–Cl5	2.6778(12)	2.6802(11)	3.1210(11)
Sb1–Cl6	2.8870(15)	2.8934(13)	2.8416(12)
Sb2–Cl11	2.6096(15)	2.6057(14)	2.4388(11)
Sb2–Cl12	2.4097(14)	2.4105(13)	2.4751(11)
Sb2–Cl13	2.4083(14)	2.4118(13)	2.4082(11)
Sb2–Cl4	2.6259(14)	2.6344(13)	2.9810(11)
Sb2–Cl5^{I}	3.2878(12)	3.2765(11)	2.8438(11)
Sb2–Cl6^{II}	3.0896(15)	3.0820(13)	3.2640(12)
Cl1–Sb1–Cl2	87.98(5)	87.71(4)	90.87(4)
Cl1–Sb1–Cl3	88.84(5)	89.14(4)	90.27(4)
Cl1–Sb1–Cl4	171.76(5)	171.87(4)	174.76(3)
Cl1–Sb1–Cl5	85.55(4)	85.68(4)	82.92(3)
Cl1–Sb1–Cl6	83.90(4)	83.90(4)	85.71(4)
Cl2–Sb1–Cl3	88.75(5)	88.99(4)	88.59(4)
Cl2–Sb1–Cl4	87.16(4)	87.20(4)	84.52(3)
Cl2–Sb1–Cl5	173.46(5)	173.29(4)	170.08(4)
Cl2–Sb1–Cl6	92.38(5)	92.74(4)	85.72(4)
Cl3–Sb1–Cl4	84.40(4)	84.43(4)	92.11(3)
Cl3–Sb1–Cl5	90.14(4)	89.80(4)	83.72(3)
Cl3–Sb1–Cl6	172.61(5)	172.76(4)	172.98(4)
Cl4–Sb1–Cl5	99.15(4)	99.25(3)	101.98(3)
Cl4–Sb1–Cl6	102.94(5)	102.67(4)	91.44(3)
Cl5–Sb1–Cl6	87.90(4)	87.67(4)	101.45(3)
Cl11–Sb2–Cl12	85.81(5)	85.95(4)	92.00(4)
Cl11–Sb2–Cl13	86.92(5)	86.88(4)	89.66(4)
Cl11–Sb2–Cl4	171.00(5)	170.80(4)	169.84(4)
Cl11–Sb2–Cl5^{I}	98.79(4)	98.15(4)	89.66(4)
Cl11–Sb2–Cl6^{II}	82.19(4)	81.79(4)	79.97(3)
Cl12–Sb2–Cl13	95.88(5)	95.93(5)	88.22(4)
Cl12–Sb2–Cl4	87.14(5)	86.88(4)	94.50(4)
Cl12–Sb2–Cl5^{I}	173.91(4)	174.07(4)	172.37(3)
Cl12–Sb2–Cl6^{II}	84.82(5)	84.63(4)	88.94(3)
Cl13–Sb2–Cl4	88.24(5)	88.13(4)	82.76(4)
Cl13–Sb2–Cl5^{I}	88.38(4)	88.60(4)	84.34(4)
Cl13–Sb2–Cl6^{II}	169.01(5)	168.60(4)	169.14(4)
Cl4–Sb2–Cl5^{I}	88.65(4)	89.45(3)	82.90(3)
Cl4–Sb2–Cl6^{II}	102.75(5)	103.27(4)	107.92(3)
Cl5^{I}–Sb2–Cl6^{II}	91.83(4)	91.69(3)	98.69(3)
Sb1–Cl4–Sb2	167.48(5)	167.68(5)	159.33(4)
Sb1–Cl5–Sb2^{III}	163.39(5)	163.05(4)	156.49(4)
Sb1–Cl6–Sb2^{IV}	154.36(5)	153.58(5)	157.37(4)

Symmetry codes: (^{I}) x, $-y+1$, $z+1/2$; (^{II}) x, $y+1$, z; (^{III}) x, $-y+1$, $z-1/2$; (^{IV}) x, $y-1$, z

Table 4
The hydrogen bond geometries (Å, deg) for DMACA at 100 and 15 K, and for TMACA at 15 K

D–H···A	D–H	H···A	D···A	D–H···A
DMACA, 100 K				
N1A–H2A···Cl5	0.88(3)	2.38(3)	3.250(5)	167(5)
N1A–H1A···Cl11^{I}	0.89(3)	2.43(4)	3.263(5)	156(5)
N2A–H9A···Cl2^{II}	0.89(3)	2.57(4)	3.377(4)	150(5)
N2A–H10A···Cl6	0.89(3)	2.91(5)	3.474(5)	123(4)
N2A–H10A···Cl11^{III}	0.89(3)	2.40(4)	3.162(4)	144(5)
N3B–H2B···Cl1^{IV}	0.89(3)	2.94(5)	3.379(5)	112(4)
N3B–H1B···Cl2	0.88(3)	2.50(3)	3.334(5)	157(5)
N3B–H2B···Cl6^{IV}	0.89(3)	2.35(3)	3.210(5)	163(5)
C1A–H5A···Cl4^{V}	0.95(3)	2.82(3)	3.718(5)	159(5)
C2A–H6A···Cl2^{VI}	0.95(3)	2.69(3)	3.631(7)	171(5)
DMACA, 15 K				
N1A–H2A···Cl5	0.88(3)	2.38(3)	3.241(5)	167(5)
N1A–H1A···Cl11^{I}	0.87(3)	2.47(4)	3.259(5)	150(5)
N2A–H9A···Cl2^{II}	0.88(3)	2.57(4)	3.375(4)	152(5)
N2A–H10A···Cl6	0.88(3)	2.89(5)	3.417(4)	121(4)
N2A–H10A···Cl11^{III}	0.88(3)	2.39(4)	3.157(4)	146(5)
N3B–H2B···Cl1^{IV}	0.88(3)	2.96(5)	3.369(4)	110(4)
N3B–H1B···Cl2	0.88(3)	2.52(3)	3.338(4)	155(5)
N3B–H2B···Cl6^{IV}	0.88(3)	2.35(3)	3.206(4)	165(5)
C1A–H5A···Cl4^{V}	0.96(3)	2.81(3)	3.697(5)	153(4)
C2A–H6A···Cl2^{VI}	0.96(3)	2.70(3)	3.643(6)	169(5)
TMACA, 15 K				
N1A–H1A···Cl5	0.85(4)	2.35(4)	3.191(4)	175(6)
N2A–H11A···Cl6	0.85(4)	2.31(4)	3.149(4)	167(5)
N3B–H1B···Cl4	0.86(4)	2.57(5)	3.274(4)	140(5)
N3B–H1B···Cl13	0.86(4)	2.82(5)	3.469(4)	134(4)
C2A–H6A···Cl11^{I}	0.95(3)	2.80(5)	3.514(6)	133(5)
C7B–H3B···Cl1^{IV}	0.95(3)	2.66(3)	3.569(5)	161(5)
C7B–H4B···Cl2	0.94(3)	2.76(3)	3.681(5)	166(5)

Symmetry codes: (^{I}) $x-1$, $-y+1$, $z-1/2$; (^{II}) $x+1$, y, z; (^{III}) x, $y-1$, z; (^{IV}) x, $-y$, $z+1/2$; (^{V}) x, $-y+1$, $z-1/2$; (^{VI}) x, $-y$, $z-1/2$

result, with the N3B cation being adequately modeled by a single well-resolved $[(CH_3)_3NH]^+$ ion whose displacement parameters are similar to those of the N1A and N2A cations that are ordered. Similarly, our new results at 100 and 15 K for DMACA show for the first time that the N2A dimethylammonium cation (in a previous paper [27] this cation was labeled N3) is well-ordered at both temperatures, again with similar displacement parameters to the cations in the N1A and N3B positions in this structure. In all three structures all of the bond lengths and angles of the di- and trimethylammonium cations are similar to those found in other low-temperature structures [29–32]. This last step in the ordering of the di-/trimethylammonium cations does not, however, lead to any further change of the symmetry because they occupy general positions in space group *Pc*.

Thus, in each of the two structures there are at least two separate ordering processes for the cations whose critical temperatures are related both to the type of cation and to the strength of H-bonding between the cations and the anionic framework. It is apparent from the structures, especially in the case of TMACA, that the N1A and N2A cations are more strongly bonded than the corresponding N3B cations (Table 4). Additionally, the ordering of the orientations of the organic cations is associated with formation of stronger and new

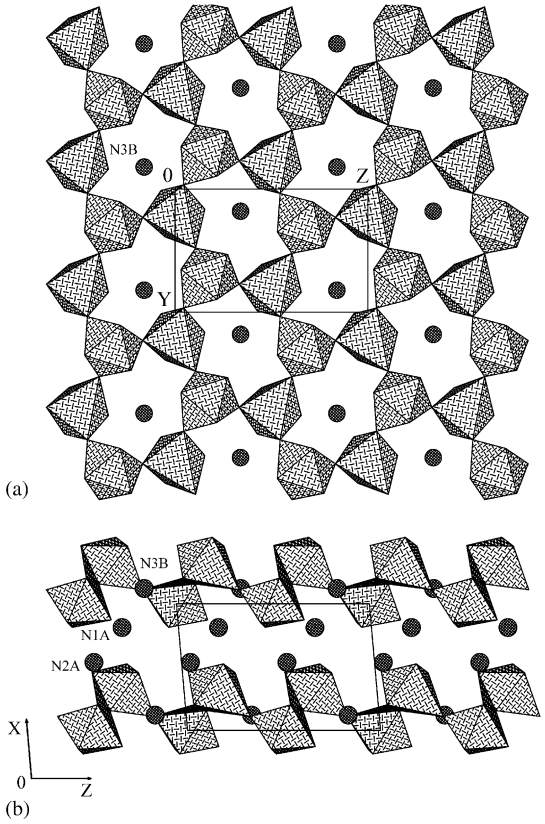

Fig. 2. A polyhedral representation of the polyanionic corrugated $[\{Sb_2Cl_9\}_n]^{3n-}$ layers built of characteristic six-membered $[Sb_6Cl_{27}]^{9-}$ rings in the structure of DMACA, at 15 K along the *a* (a) and *b* (b) axes. The positions of the dimethylammonium cations are shown by circles.

hydrogen bonds between the organic cations and inorganic layers.

3.3. Inorganic anionic framework

There are two crystallographically non-equivalent antimony(III) atoms in both compounds, each of which is octahedrally coordinated. The $[SbCl_6]^{3-}$ octahedra share corners to form characteristic six-membered $[Sb_6Cl_{27}]^{9-}$ rings, which are in turn connected to each other to form polyanionic corrugated $[\{Sb_2Cl_9\}_n]^{3n-}$ layers parallel to the (100) planes of the crystals (Fig. 2). The overall pattern of distortions and geometry of the Sb–Cl bond lengths and Cl–Sb–Cl angles within these anionic layers at 100 and 15 K are similar to those found at higher temperatures as well as other chloroantimonates(III) containing the same anionic layers [5,14,18,27,28,33,34]. The only difference is that one out of the three bridging chlorine atoms was found to be disordered in the structure of TMACA at 373 K. Its position is split between two sites with half occupancy [28].

In both compounds the $[SbCl_6]^{3-}$ octahedra occupy general positions in the structures of both the paraelectric and ferroelectric phases. Their geometry is therefore not constrained by symmetry and all six Sb–Cl bonds within an octahedron can be of different lengths. A measure of the distortion of each octahedron from regularity is provided by the distortion parameters for bond-length $\Delta = 1/6\sum_{i=1}^{6}[(\overline{R}_i - \overline{R})/\overline{R}]^2$, ($\bar{R}$ is the average Sb–Cl bond length within the octahedron and the R_i are the individual Sb–Cl bond lengths of the octahedron) and bond-angle $\sigma^2 = 1/11\sum_{i=1}^{12}(\alpha_i - 90^\circ)^2$ (α_i is the individual *cis* Cl–Sb–Cl bond angle of the octahedron) [35,36]. The distortion parameters for the structures of DMACA and TMACA at different temperatures (Table 5) show that the $[SbCl_6]^{3-}$ octahedra in the structure of TMACA are more distorted than in DMACA. Further, the bond length distortion parameters of the octahedra for DMACA structures increase during cooling through the para-ferroelectric phase transition, and then subsequently decrease on further cooling in the ferroelectric phase. The σ^2 parameters for these structures clearly increase with decreasing temperature. The Δ parameters calculated for the polyhedra in TMACA structures, in general, decrease with decreasing temperature, whereas σ^2 parameters increase.

The distortions of the $[SbCl_6]^{3-}$ octahedra in the structures of DMACA and TMACA are due to two major influences. First, comparison of the observed Sb–Cl bond lengths and Cl–Sb–Cl angles with an isolated $[SbCl_6]^{3-}$ octahedron found in the structure of $[Co(NH_3)_6][SbCl_6]$ [37], clearly shows that the deformations of the inorganic layers in both compounds are mainly related to the condensation of the octahedra and the sharing of Cl atoms between them. Thus, while the Sb–Cl bond lengths of the isolated $[SbCl_6]^{3-}$ octahedron of $[Co(NH_3)_6][SbCl_6]$ are 2.643(6) Å (2.652(6) Å when corrected assuming a riding model), the average Sb–Cl bond lengths in DMACA at 100 K for the Sb1 and the Sb2 octahedra are, respectively, 2.7037 and 2.7385 Å (Table 3). At 15 K the deviations from 2.652(6) Å are somewhat smaller: the average Sb–Cl distances are 2.7026 (Sb1) and 2.7368 Å (Sb2 octahedron). In TMACA at 15 K the average Sb–Cl bond lengths in both octahedra are considerably longer at 2.7419 and 2.7352 Å. This average expansion of the $[SbCl_6]^{3-}$ octahedra is a result of the Sb–Cl bonds to the bridging Cl atoms being up to 0.6 Å longer than those in $[Co(NH_3)_6][SbCl_6]$, while the bonds to the non-bridging Cl are only ~0.1–0.2 Å shorter. The resulting differences between the shortest and the longest Sb–Cl bonds are 0.7664 and 0.8795 Å at 100 K, and 0.7395 and 0.8660 Å at 15 K for the Sb1 and Sb2 octahedra in DMACA. The anionic structure of TMACA crystal at 15 K is somewhat more distorted than that of the dimethylammonium analogue (Table 3, Fig. 3). The terminal Sb–Cl distances for both octahedra are between 2.4036(11) and 2.4888(11) Å, whereas the bridging ones vary from 2.8416(11) to 3.2640(12) Å. The largest difference in

Table 5
The calculated octahedral distortion parameters Δ and σ^2 for independent Sb1 and Sb2 octahedra in the DMACA and TMACA crystals at different temperatures

DMACA						
Temperature (K)			298	200	100	15
		Bond-length distortion parameter $\Delta \times 10^3$				
Sb1	Octahedron		9.52	10.35	9.45	8.96
Sb2				14.22	14.92	14.47
		Bond-angle distortion parameter σ^2				
Sb1	Octahedron		22.7	30.8	33.2	32.8
Sb2				32.0	37.1	38.0
TMACA						
Temperature (K)		373	295	165	95	15
		Bond-length distortion parameter $\Delta \times 10^3$				
Sb1	Octahedron	13.89/16.80[a]	14.99	14.78	14.46	14.05
Sb2			15.19	14.33	13.96	13.69
		Bond-angle distortion parameter σ^2				
Sb1	Octahedron	20.9/51.5[a]	33.7	36.6	38.1	40.0
Sb2			40.3	54.1	57.0	60.1

[a]The two values for TMACA at 373 K are calculated for the two sites occupied by the disordered Cl5 atom [28].

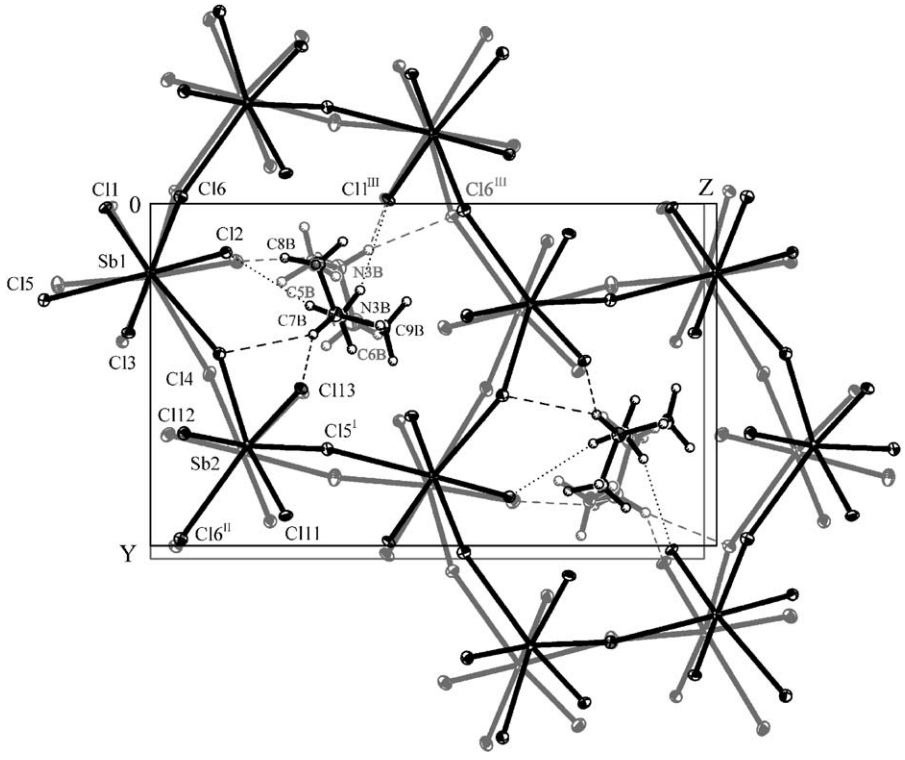

Fig. 3. The superimposed anionic layers of DMACA (gray) and TMACA (black) crystals with organic cations embedded inside the $[Sb_6Cl_{27}]^{9-}$ rings at 15 K along their *a*-axes. The dashed and dotted lines indicate N–H···Cl and C–H···Cl hydrogen bonds, respectively. Displacement ellipsoids are plotted at the 50% probability level. Symmetry codes: (^{I}) x, $-y+1$, $z+1/2$; (^{II}) x, $y+1$, z; (^{III}) x, $-y$, $z+1/2$.

Sb–Cl distances (0.8558 Å) within the same octahedron was found for the Sb2 polyhedron. The three bridging Sb–Cl bonds are mutually *cis* to each other for both Sb1 and Sb2 octahedra in both DMACA and TMACA. These Cl(br)–Sb–Cl(br) angles are mostly increased from the 90° they would have in an undistorted octahedron, while the Cl(*t*)–Sb–Cl(*t*) (*t*—terminal) angles remain in the range 86–96°, similar to the average Cl–Sb–Cl angle of 90.9(2)° in the isolated octahedron of $[Co(NH_3)_6][SbCl_6]$ [37].

The secondary cause of deformation of the $[SbCl_6]^{3-}$ octahedra in these compounds is weaker than the

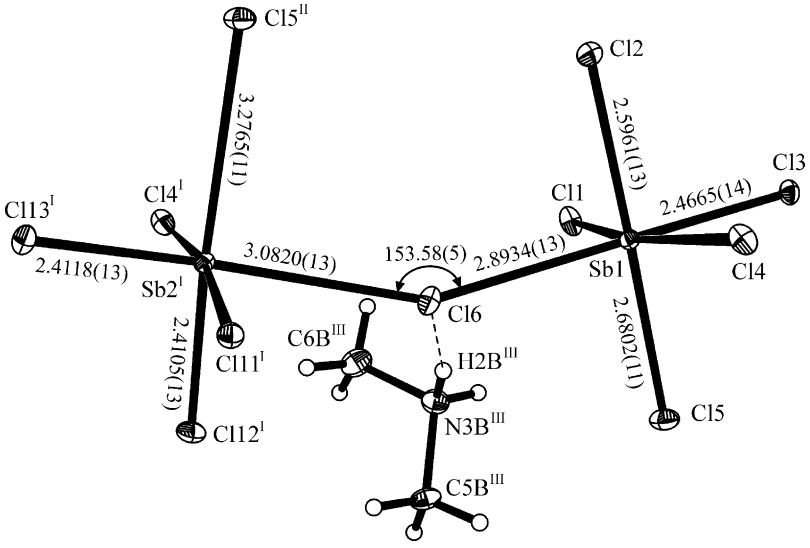

Fig. 4. The N2B^{III}–H2B^{III}···Cl6 hydrogen bond (indicated by the dashed line) partly causing the deformation of Sb1–Cl6–Sb2^{I} angle in the structure of DMACA, at 15 K. Displacement ellipsoids are plotted at the 50% probability level. Symmetry codes: (^{I}) x, y–1, z; (^{II}) x, –y, z+1/2, (^{III}) x, –y, z–1/2.

primary one, and is caused by the differences in geometry and strength of interactions between the anionic layers and the organic cations. In the purely inorganic compound α-$Cs_3[Sb_2Cl_9]$ chloroantimonate(III), in which there are no hydrogen bonds, the two independent Sb–Cl bond lengths are 2.42 and 2.82 Å (average 2.62 Å), *cis* Cl–Sb–Cl bond angles vary from 85.9 to 95.0° (average 89.9°) and the inter-octahedral Sb–Cl–Sb angle is 170.8° [38,39]. The formation of hydrogen bonds between the cations and all of the chlorine atoms except the non-bridging Cl3, Cl12 and Cl13 in DMACA results in the displacement of the chlorine atoms towards the organic cations [40], and especially the reduction of Sb–Cl–Sb bond angles (Table 3). At 200 K the N2A dimethylammonium cation (N3 in a previous paper [27]) is disordered so there is no hydrogen bond between the cation and Cl6 and the Sb1–Cl6–Sb2^{IV} angle (Sb1–Cl4–Sb2^{I}, (^{I}) x, y–1, z in reference [27]) is 157.0°. At 15 K the cation is ordered and the formation of the N2A···Cl6 hydrogen bond, along with the shortening of the N3B–H2B···Cl6^{IV} interaction (N1–H1B···Cl4 in Ref. [27]) from 3.25(1) to 3.206(4) Å results in a decrease in the Sb1–Cl6–Sb2^{IV} angle of 3.42° ([27], Tables 3 and 4). The geometries of the hydrogen bonds in DMACA are similar at 100 and 15 K because there is no change in the ordering of the cations. The D···A distances are between 3.157(4) and 3.718(5) Å, whereas the D–H···A angles vary from 110(4) to 171(5)° (Table 4). Among the N–H···Cl interactions, the largest change on lowering temperature in N···Cl distances, 0.057 Å, occurs for N2A–H10A···Cl6 hydrogen bond. It results in the change in the Sb1–Cl6–Sb2^{IV} angle, which decreases from 154.36(5)° at 100 K to 153.58(5)° at 15 K (Tables 3 and 4, Fig. 4).

A comparison of the geometries of the anionic layers of TMACA and DMACA at 15 K also indicates the strength of the influence of the hydrogen bonding, especially on the bridging Cl–Sb–Cl and Sb–Cl–Sb inter-octahedral angles (Tables 3 and 4, Fig. 3). The largest difference in Sb–Cl–Sb angles (8.35°) is for Sb1–Cl4–Sb2. It results from the presence of the stronger N3B–H1B···Cl4 hydrogen bond in the structure of TMACA than the C1A–H5A···Cl4^{V} interaction found in the DMACA crystal.

4. Summary and concluding remarks

The structures of $[(CH_3)_2NH_2]_3[Sb_2Cl_9]$ (DMACA) and $[(CH_3)_3NH]_3[Sb_2Cl_9]$ (TMACA) crystals were determined by single crystal X-ray diffraction down to 15 K. Both compounds exhibit the *Pc* space group at both 100 and 15 K. The new data for DMACA show that at 100 K one of the crystallographically independent dimethylammonium cations, previously found to be disordered in the structure at 200 K [27], was ordered. On the basis of this result we can now suggest that the changes in the infra-red and NMR spectra of this compound observed in the temperature range of 105–140 K [23,24] are probably related to the ordering of the orientation of this third cation. The analogous ordering process occurs in TMACA above 165 K (Fig. 1). As a result of the ordering, new and somewhat stronger hydrogen bonds are formed, as previously reported for TMACA [5]. These hydrogen bonds, as well as the inter-ionic interactions, cause a deformation of the inorganic $[SbCl_6]^{3-}$ octahedra. On decreasing temperature, in general for both compounds, the bond-length distortion parameters of $[SbCl_6]^{3-}$ octahedra

decrease whereas the bond-angle parameters clearly increase. NMR measurements indicate that the dynamic flipping of the individual methyl groups around the N–C bonds present from high temperatures [21] becomes suppressed at around 125 K in TMACA [20,22] and possibly around 80 K in DMACA [23]. The fact that we do not detect any significant structural response of the framework to this freezing is consistent with the interactions between the methyl hydrogen atoms and the anionic framework being weak or absent. Our data at 15 K, in agreement with the results of pyroelectric studies [41], do, however, rule out the suggestion by Varma et al. [24] that the changes they report in infrared and Raman spectra at temperatures below 150 K in both compounds are due to a further reduction in symmetry. Our suggestion is that the changes in the spectra are, instead, a splitting of bands as a consequence of increasing differences between the environments of chemically equivalent but symmetrically distinct cations.

At the present stage of knowledge about DMACA and TMACA crystals the relative role of the inter-ionic interactions and the dynamics of the organic cations in determining the structural evolution is not yet fully determined. Clearly, one of the distinguishing features of these structures is the presence on the Sb^{III} atom of an electron lone-pair, which presumably contributes to a flexibility of the anionic architecture and its resulting ability to adapt to the size and symmetry of various organic cations. The dynamics of the cations are clearly influenced by the formation of hydrogen bonds to the anionic framework, but the role of the feedback from the framework in determining the strength of the H-bonding and the barrier to the reorientation of the organic cations has yet to be determined. One possibility to obtain separation of these effects is to extend the previous high-pressure [42,43], low-temperature studies [5,27] by single-crystal high-pressure diffraction studies of compounds such as DMACA that possess disordered cations at room temperature. Such studies will be used to probe the balance between the inter- and intramolecular forces that appear to control the polar properties as well as the phase transition behavior of those compounds.

Acknowledgments

This material is based upon work supported by the North Atlantic Treaty Organization under a grant awarded in 2004 (DGE-0410297). We acknowledge financial support from the National Science Foundation (CHE-0131128) for the purchase of the Oxford Diffraction Xcalibur 2 single-crystal diffractometer. The authors are grateful to Dr. C. Slebodnick (Department of Chemistry, Virginia Tech), Dr. N. Vogelaar (Department of Biology, Virginia Tech) and Mr. D. Warner (Oxford Diffraction Ltd.) for valuable discussions and help during the low-temperature X-ray experiment. We thank Prof. B. Hanson (Department of Chemistry, Virginia Tech) for providing the starting materials and opportunity to prepare crystals in his laboratory.

References

[1] G.A. Fischer, N.C. Norman, Adv. Inorg. Chem. 41 (1994) 233–271.
[2] J. Zaleski, Structure, Phase Transitions and Molecular Motions in Chloroantimonates(III) and Bismuthates(III), Opole University Press, Opole, Poland, 1995.
[3] L. Sobczyk, R. Jakubas, J. Zaleski, Polish J. Chem. 71 (1997) 265–300.
[4] M. Bujak, Ph.D. Thesis, University of Opole, Opole, Poland, 2000.
[5] M. Bujak, J. Zaleski, J. Solid State Chem. 177 (2004) 3202–3211.
[6] R. Jakubas, L. Sobczyk, Phase Trans. 20 (1990) 163–193.
[7] G. Bator, J. Baran, R. Jakubas, L. Sobczyk, J. Mol. Struct. 450 (1998) 89–100.
[8] R. Jakubas, G. Bator, Z. Ciunik, Ferroelectrics 295 (2003) 3–8.
[9] H. Ishihara, K. Watanabe, A. Iwata, Y. Yamada, Y. Kinoshita, T. Okuda, V.G. Krishnan, S. Dou, A.Z. Weiss, Z. Naturforsch. 47a (1992) 65–74.
[10] R. Jakubas, U. Krzewska, G. Bator, L. Sobczyk, Ferroelectrics 77 (1988) 129–135.
[11] R. Jakubas, Z. Galewski, L. Sobczyk, J. Matuszewski, J. Phys. C 18 (1985) L857–L860.
[12] R. Jakubas, G. Bator, J. Mróz, Ferroelectrics 146 (1993) 65–71.
[13] A. Iwata, M. Eguchi, Y. Ishibashi, S. Sasaki, H. Shimizu, T. Kawai, S. Shimanuki, J. Phys. Soc. Jpn. 62 (1993) 3315–3326.
[14] M. Gdaniec, Z. Kostrukiewicz, R. Jakubas, L. Sobczyk, Ferroelectrics 77 (1988) 31–37.
[15] R. Jakubas, L. Sobczyk, J. Matuszewski, Ferroelectrics 74 (1987) 339–345.
[16] R. Jakubas, Solid State Commun. 60 (1986) 389–391.
[17] G. Bator, R. Jakubas, Phys. Status Solidi A 147 (1995) 591–600.
[18] A. Kallel, J.W. Bats, Acta Crystallogr. C 41 (1985) 1022–1024.
[19] R. Jakubas, Z. Czapla, Z. Galewski, L. Sobczyk, Ferroelectrics Lett. 5 (1986) 143–148.
[20] S. Idziak, R. Jakubas, Solid State Commun. 62 (1987) 173–175.
[21] S. Urban, W. Zając, R. Jakubas, C.J. Carlile, B. Gabryś, Physica B 180 & 181 (1992) 1050–1052.
[22] B. Jagadeesh, P.K. Rajan, K. Venu, V.S.S. Sastry, Solid State Commun. 86 (1993) 803–806.
[23] B. Jagadeesh, P.K. Rajan, K. Venu, V.S.S. Sastry, Solid State Commun. 91 (1994) 843–847.
[24] V. Varma, R. Bhattacharjee, H.N. Vasan, C.N.R. Rao, Spectrochim. Acta 48A (1992) 1631–1646.
[25] Oxford Diffraction; CrysAlis CCD, Data collection GUI for CCD and CrysAlis RED, CCD data reduction GUI versions 1.171.24 beta (release 23.09.2004), Oxford Diffraction, Poland, 2004.
[26] G.M. Sheldrick, SHELXTL NT, 6.12, Bruker Analytical X-ray Systems, Inc., Madison, WI, USA, 2001.
[27] J. Zaleski, A. Pietraszko, Acta Crystallogr. B 52 (1996) 287–295.
[28] M. Bujak, J. Zaleski, Cryst. Eng. 4 (2001) 241–252.
[29] M. Bujak, J. Zaleski, Acta Crystallogr. C 54 (1998) 1773–1777.
[30] F. Knödler, U. Ensinger, W. Schwarz, A. Schmidt, Z. Anorg. Allg. Chem. 557 (1988) 208–218.
[31] I.D. Williams, P.W. Brown, N.J. Taylor, Acta Crystallogr. C 48 (1992) 259–263.

[32] G. Chapuis, F.J. Zuniga, Acta Crystallogr. B 36 (1980) 807–812.
[33] F.J. Kruger, F. Zettler, A. Schmidt, Z. Anorg. Allg. Chem. 449 (1979) 135–144.
[34] J. Zaleski, to be published.
[35] I.D. Brown, R.D. Shannon, Acta Crystallogr. A 29 (1973) 266–282.
[36] K. Robinson, G.V. Gibbs, P.H. Ribbe, Science 172 (1971) 567–570.
[37] D.R. Schroeder, R.A. Jacobson, Inorg. Chem. 12 (1973) 210–213.
[38] K. Kihara, T. Sudo, Z. Kristallogr. 134 (1971) 142–144.
[39] K. Kihara, T. Sudo, Z. Kristallogr. 134 (1971) 155–158.
[40] M. Bujak, J. Zaleski, Z. Naturforsch. 57b (2002) 157–164.
[41] R. Jakubas, J. Mróz, P. François, J. Lefebvre, Ferroelectrics 173 (1995) 221–231.
[42] M. Zdanowska-Frączek, R. Jakubas, M. Krupski, J. Phys. Chem. Solids 65 (2004) 1679–1682.
[43] M. Zdanowska-Frączek, R. Jakubas, M. Krupski, Ferroelectrics 302 (2004) 91–93.